

## Supplementary Information:

# Hybrid PEDOT/MnO<sub>x</sub> nanostructured electrocatalysts for oxygen reduction

*Julian A. Vigil, Timothy N. Lambert,\* Maria Kelly and Ruby Aidun*

Department of Materials, Devices, and Energy Technologies, Sandia National  
Laboratories, Albuquerque, NM, USA, 87185.

\*Corresponding author: Tel: 505 284 6967; E-mail: [tnlambe@sandia.gov](mailto:tnlambe@sandia.gov).

Supporting Information (9 pp.)

### Table of Contents

Experimental Methods	S-2
Fig. S1	S-4
Fig. S2	S-5
Fig. S3	S-6
Fig. S4	S-7
Fig. S5	S-8
Fig. S6	S-9

## Experimental Methods

### Materials Characterization

*Quartz Crystal Microbalance (QCM):* PEDOT mass deposition rates, as well as the rate of MnO<sub>x</sub> uptake, were monitored using an Inficon Maxtek RQCM connected to a Solartron SI1287 Potentiostat, operated by Corrware and RQCM Data Logging Software. Galvanostatic electropolymerization was performed as described above, where the working electrode was a polished 1 in. diameter, 9 MHz Ti/Pt quartz crystal electrode. Following the EDOT electropolymerization step to form PEDOT, the crystal holder was quickly transferred to a DI H<sub>2</sub>O wash bath, then to the KMnO<sub>4</sub> solution while the frequency was monitored throughout. The QCM capacitance cancellation was confirmed once the crystal was transferred from acetonitrile to aqueous solution. Mass change was calculated using the crystal's measured frequency change and the Sauerbrey equation.

*X-ray photoelectron spectroscopy (XPS):* PEDOT, P-MnO<sub>x</sub>-10, P-MnO<sub>x</sub>-20, and P-MnO<sub>x</sub>-30 films on silica-supported GC electrodes were analyzed directly. Spectra were collected using a Kratos AXIS Ultra DLD photoelectron spectrometer with a monochromatic Al K $\alpha$  (1486.7 eV) source. The analysis area was an elliptical spot size of 300 x 700 microns. Several locations on each sample were analyzed to obtain a representative sampling. Survey spectra were recorded at pressures less than  $5 \times 10^{-9}$  Torr with 80 eV pass energy, 500 meV step sizes, and 100 ms dwell times. High resolution spectra were recorded with a 20 eV pass energy, 50 meV step sizes, and 100 ms dwell times. Data processing was performed with CasaXPS Version 2.3.15. High-resolution core-level peaks were compared by normalizing counts for each respective core-level.

*Focused-ion beam (FIB), scanning electron microscopy (SEM), and energy dispersive spectroscopy (EDS):* Films grown on silica-supported GC electrodes were imaged using a Zeiss Supra 55VP field emitter gun scanning electron microscope (FEGSEM). Elemental analysis by SEM was collected using the Zeiss Supra 55VP as the X-ray source and a Bruker SSD as the collector. Spectra were collected using the Bruker Esprit 2.0 software.

*Fourier transform infrared (FTIR) spectroscopy:* Spectra were collected on a Nicolet NEXUS 870 FTIR using a PIKE MIRacle ATR attachment. Films deposited on pyrolyzed carbon (on fused silica) substrates were placed face down on the ATR crystal and typical data collection averaged 40 scans between 480 - 4000 cm<sup>-1</sup> with a resolution of 2 cm<sup>-1</sup>.

Blank pyrolyzed carbon substrates and a PEDOT film was used for background subtraction.

### Electrochemical Characterization

Based on QCM measurements of the PEDOT film deposition ( $20\text{ s}$ ,  $1\text{ mA cm}^{-2}$ ) and  $\text{MnO}_x$  uptake, film mass loadings on the RDE GC working electrodes were calculated: PEDOT,  $20.66 \pm 1.85\ \mu\text{g cm}^{-2}$ ; P-MnOx-10,  $28.28 \pm 3.13\ \mu\text{g cm}^{-2}$ ; P-MnOx-20,  $30.6 \pm 3.35\ \mu\text{g cm}^{-2}$ ; P-MnOx-30,  $32.17 \pm 3.55\ \mu\text{g cm}^{-2}$ . An ink of  $0.62\text{ mg}$  20% Pt/C powder,  $1.095\text{ mL}$  DI  $\text{H}_2\text{O}$ ,  $0.292\text{ mL}$  *i*-PrOH and  $0.073\text{ mL}$  Nafion solution was sonicated for  $20\text{ min}$ , and  $5\ \mu\text{L}$  of the ink was drop-cast onto an identical ( $A = 0.0707\text{ cm}^2$ ) RDE GC working electrode ( $30\ \mu\text{g cm}^{-2}$ ).

RDE experiments were carried out using a RDE-2 three-electrode cell with a rotating working electrode (Bioanalytical Systems, Inc.), controlled by a VersaSTAT 4 potentiostat (Princeton Applied Research) and the VersaStudio software suite. The three-electrode cell included the glassy carbon/catalyst film rotating working electrode, Ag/AgCl (3 M NaCl,  $0.196\text{ V vs NHE}$ ) reference electrode and Pt coil counter electrode. Hydrodynamic linear scanning voltammetry (LSV), cyclic voltammetry (CV), and electrochemical impedance spectroscopy (EIS) methods were used to assess the catalysts' ORR properties. LSV scans were collected scanning from  $0.1\text{ V}$  to  $-0.7\text{ V vs Ag/AgCl}$  at a scan rate of  $5\text{ mV s}^{-1}$  at rotation rates of 500, 900, 1600, 2500 and 3600 RPM. Identical LSVs were collected in Ar-sat. electrolyte, and the measured background currents were subtracted from the measured ORR current in  $\text{O}_2$ -sat. electrolyte. Static CV experiments were conducted by scanning from  $0.1$  to  $-0.7\text{ V vs Ag/AgCl}$  at a scan rate of  $50\text{ mV s}^{-1}$  in  $\text{O}_2$ -sat. electrolyte and Ar-sat. electrolyte. Potentiostatic EIS spectra were collected in the onset and half-wave regions of the obtained LSV curves, by scanning frequency from  $10^5$  to  $10^{-1}\text{ Hz}$  with  $10\text{ mV RMS}$  amplitude perturbations.

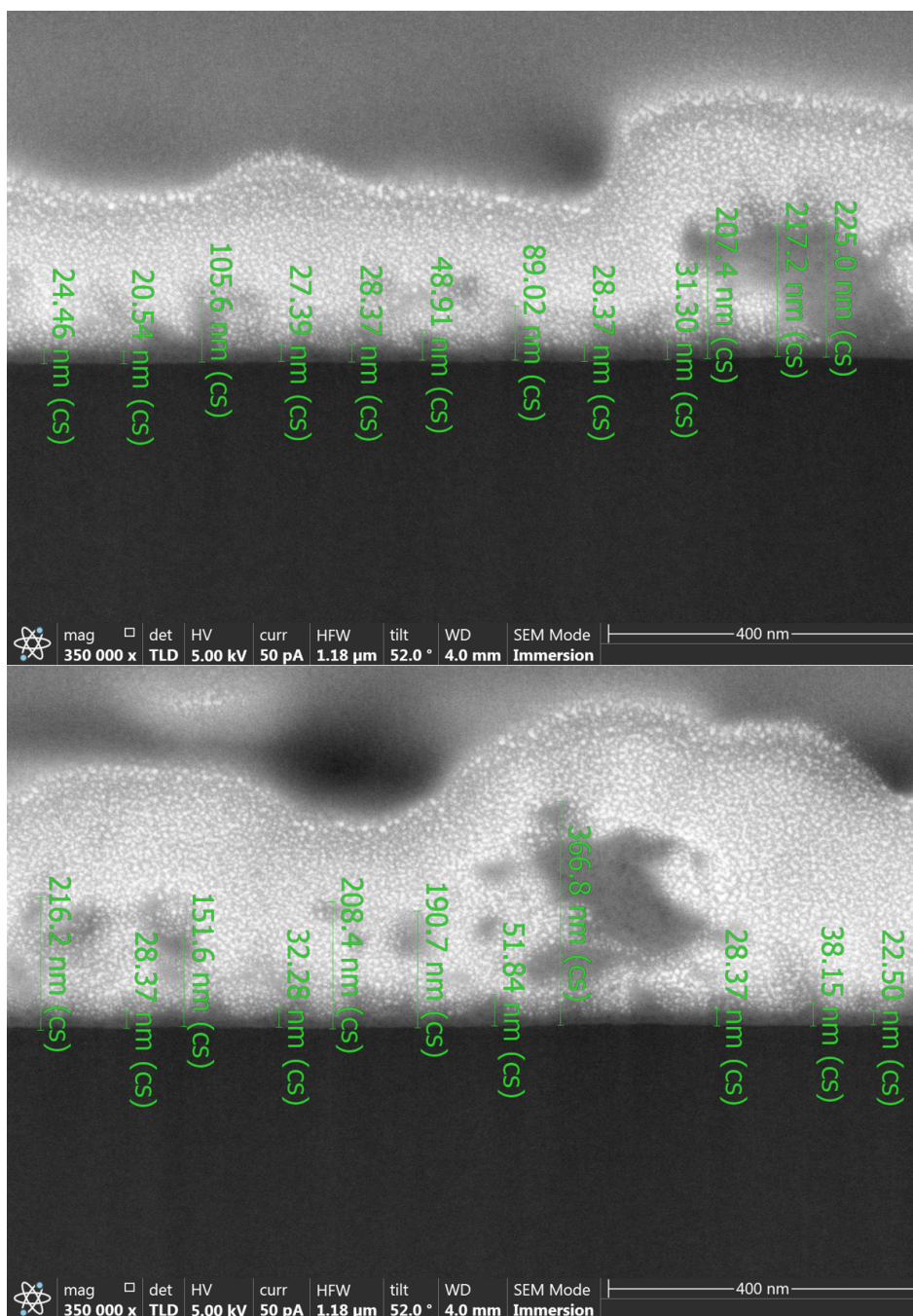


**Fig. S1.** FIB/SEM cross-sectional analysis of a P-MnO<sub>x</sub>-20 film on a glassy carbon electrode. Films were imaged on the electrode with an E-beam deposited Pt layer for protection and I-beam deposited C overcoat to protect the surface. Images were collected at an angle and corresponding tilt correction has been applied to the measurements, which show values ranging from 20.54 nm to 366.8 nm. The bulk of the film ranges in thickness from 20 – 70 nm, with the larger particulates reaching as much as *ca.* 367 nm from the surface of the GC electrode.

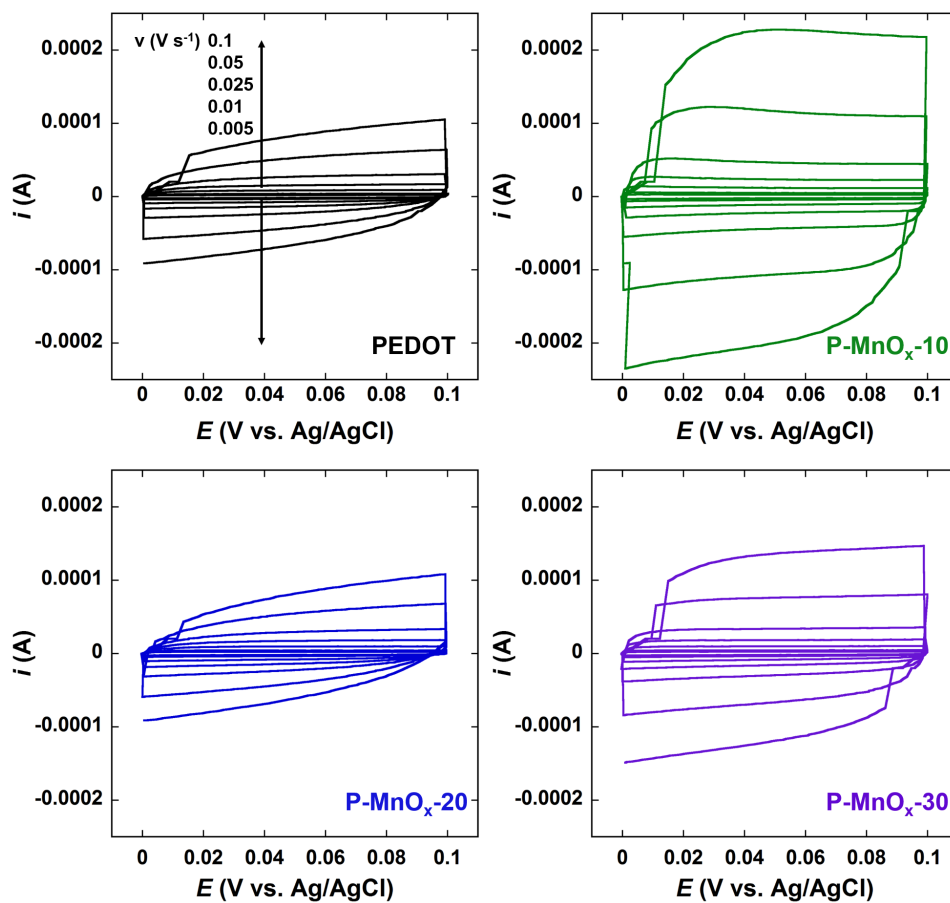


**Fig. S2.** CV scans at increasing scan rate in a non-Faradaic potential window for the determination of the double-layer capacitance. The scan rate was increased from 0.005 to 0.01 to 0.025 to 0.05 to 0.1  $\text{V s}^{-1}$  corresponding to an increasing in the capacitive current.

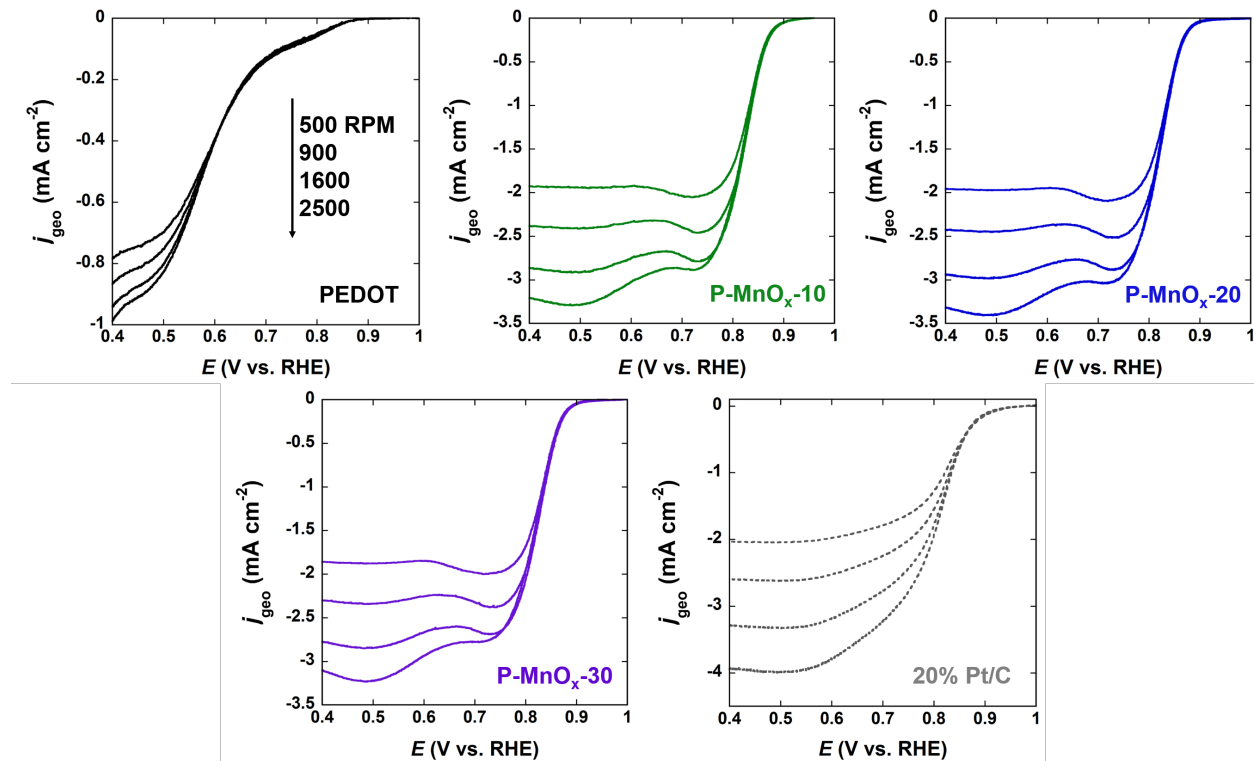


**Fig. S3.** Full background-subtracted RDE LSV scans at all rotation rates in 0.1 M KOH electrolyte for Koutecky-Levich analysis, with diffusion-limited current density increasing as rotation rate increases from 500 to 900 to 1600 to 2500 RPM. Average catalyst mass loading: PEDOT,  $20.8 \mu\text{g cm}^{-2}$ ; P-MnO<sub>x</sub>-10,  $28.3 \mu\text{g cm}^{-2}$ ; P-MnO<sub>x</sub>-20,  $30.6 \mu\text{g cm}^{-2}$ ; P-MnO<sub>x</sub>-30,  $32.2 \mu\text{g cm}^{-2}$ ; 20% Pt/C,  $30.0 \mu\text{g cm}^{-2}$ .

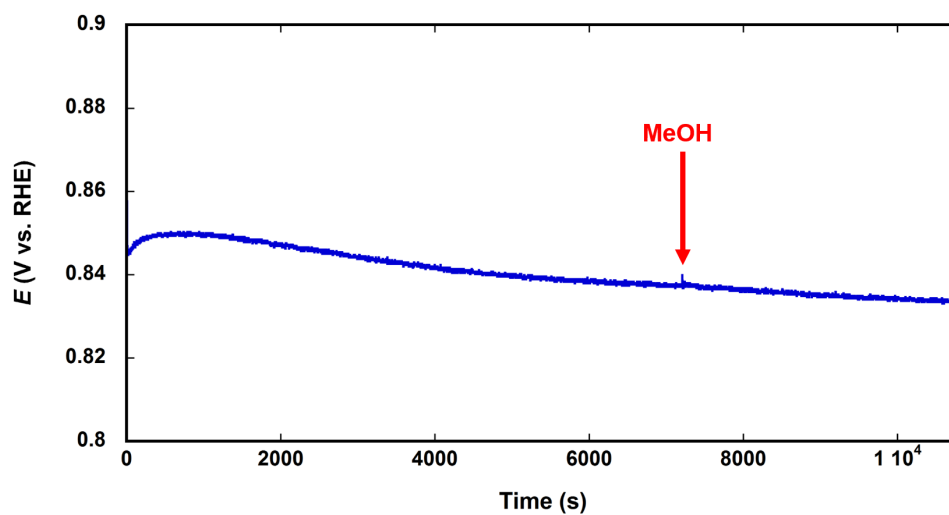


**Fig. S4.** Chronopotentiometric response of a  $80 \mu\text{g cm}^{-2}$  P-MnO<sub>x</sub>-20 film at a geometric current density of  $1 \text{ mA cm}^{-2}$ . MeOH was injected into the cell after two hours to reach a concentration of 5 wt. % MeOH.

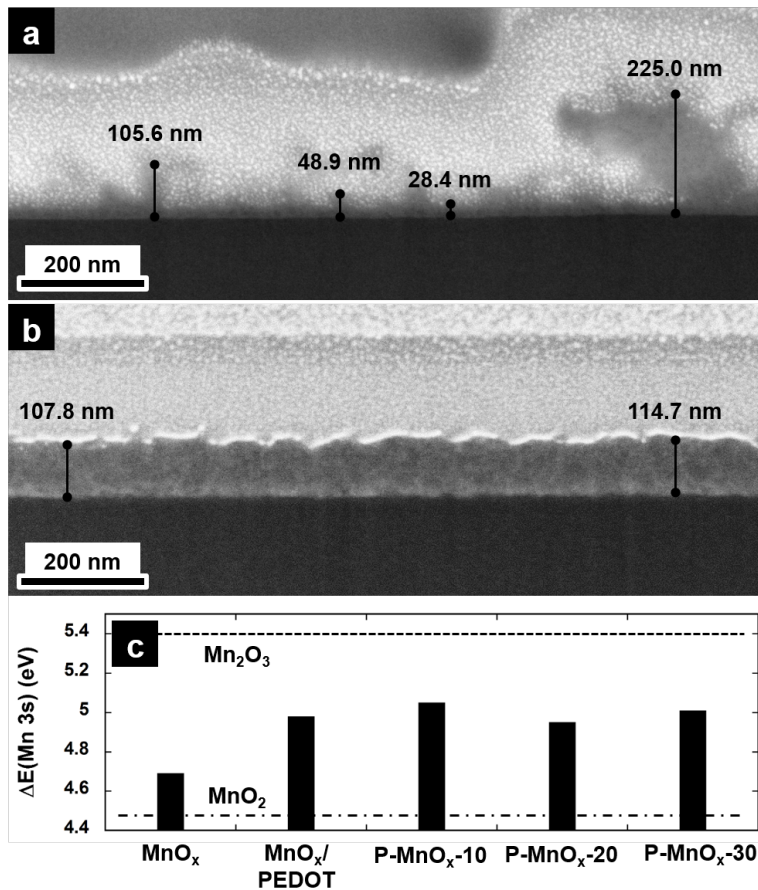


**Fig. S5.** FIB/SEM cross-sectional analysis of (a) P-MnO<sub>x</sub>-20 film, (b) MnO<sub>x</sub>/PEDOT film from the aqueous micellar co-electrodeposition approach; (c) Comparison of  $\Delta E(\text{Mn } 3s)$  values for electrodeposited MnO<sub>x</sub> and co-electrodeposited MnO<sub>x</sub>/PEDOT films (aqueous and aqueous micellar electrodepositions, respectively) relative to P-MnO<sub>x</sub>-10, P-MnO<sub>x</sub>-20, P-MnO<sub>x</sub>-30. Values for Mn<sup>III</sup><sub>2</sub>O<sub>3</sub> and Mn<sup>IV</sup>O<sub>2</sub> are represented by the horizontal lines.



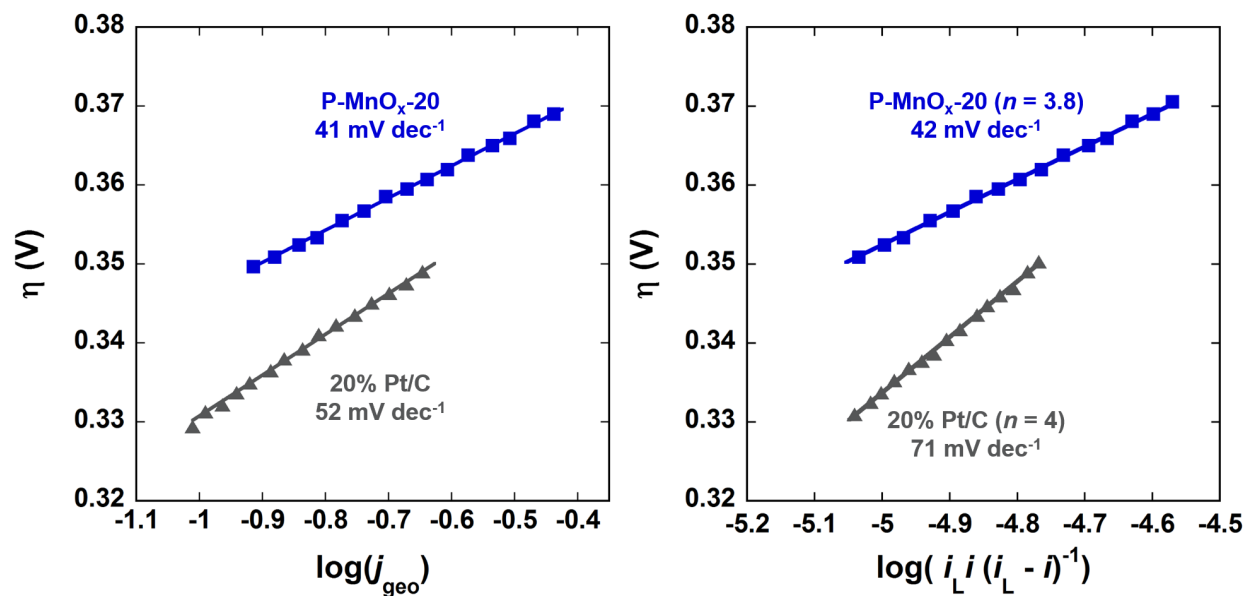


**Fig. S6.** Tafel plots and slopes for P-MnO<sub>x</sub>-20 and 20% Pt/C in the potential window  $\pm 10$  mV relative to the calculated ORR onset potential based on the LSV curves, derived from (a) geometric current density and (b) mass-transport corrected current.